

Gastruloids generated without exogenous Wnt activation develop anterior neural tissues

Mehmet U. Girgin,¹ Nicolas Broguiere,¹ Lorenzo Mattolini,¹ and Matthias P. Lutolf^{1,2,*}

¹Laboratory of Stem Cell Bioengineering, Institute of Bioengineering, School of Life Sciences and School of Engineering, École Polytechnique Fédérale de Lausanne (EPFL), 1015 Lausanne, Switzerland

²Institute of Chemical Sciences and Engineering, School of Basic Science, EPFL, 1015 Lausanne, Switzerland

*Correspondence: matthias.lutolf@epfl.ch

<https://doi.org/10.1016/j.stemcr.2021.03.017>

SUMMARY

When stimulated with a pulse from an exogenous WNT pathway activator, small aggregates of mouse embryonic stem cells (ESCs) can undergo embryo-like axial morphogenesis and patterning along the three major body axes. However, these structures, called gastruloids, currently lack the anterior embryonic regions, such as those belonging to the brain. Here, we describe an approach to generate gastruloids that have a more complete antero-posterior development. We used hydrogel microwell arrays to promote the robust derivation of mouse ESCs into post-implantation epiblast-like (EPI) aggregates in a reproducible and scalable manner. These EPI aggregates break symmetry and axially elongate without external chemical stimulation. Inhibition of WNT signaling in early stages of development leads to the formation of gastruloids with anterior neural tissues. Thus, we provide a new tool to study the development of the mouse after implantation *in vitro*, especially the formation of anterior neural regions.

INTRODUCTION

The development of the mouse embryo is an incredibly complicated and fascinating process that leads to a complete body plan with perfectly organized organs and tissues within just a few weeks. Numerous *in vivo* studies have been made to understand how this process takes place. Compared with other model organisms, however, the performance of genetic experiments on mice is often time-consuming and is complicated by the limited accessibility of the embryos after implantation. This has motivated the establishment of *in vitro* models to study early embryonic development.

The first attempts to model the embryonic development of the mouse *in vitro* began with an incidental observation. Embryonic carcinoma cells (ECCs) isolated from testicular tumors (Kleinsmith and Pierce, 1964) were aggregated *in vitro* to form so-called embryoid bodies (EBs), which recapitulated aspects of the spatial organization of mouse embryos on day 5 of development (Martin and Evans 1975). ECCs in EBs were then rapidly replaced by embryonic stem cells (ESCs) to generate cell types derived from all three germ layers (Bain et al., 1995; Boheler et al., 2002; Kubo et al., 2004). However, although countless important studies with EBs as the model system have been performed, revealing the remarkable self-organizing potential of ESCs (ten Berge et al., 2008), the lack of robustness in development, and the morphogenesis of EBs has made it difficult to study more complex aspects of embryonic development. An improved version of EBs, termed gastruloids, can be generated from smaller ESC aggregates, well-defined media, and timed chemical stimulation, resulting in a stereo-

typical *in vivo*-like axial elongation and patterning (van den Brink et al., 2014; Turner et al., 2017; Beccari et al., 2018). These multicellular aggregates were shown to recapitulate spatiotemporal activation of *Hox* genes, a phenomenon that is evolutionarily conserved among vertebrates (Mallo and Alonso 2013). Compared with the embryo, however, the development of the gastruloid is limited to the post-occipital region (Beccari et al., 2018), with anterior nervous tissues, which correspond to the forebrain, midbrain, and hindbrain, largely absent.

The derivation of mouse gastruloids is based on the treatment of mouse ESC aggregates with the WNT agonist CHIR99021, which induces symmetry breaking and axial elongation in the initial radially symmetrical structure. This leads to ubiquitous activation of WNT signaling and expression of the primitive streak marker T/BRA across the aggregate, resulting in a uniform induction of mesodermal differentiation. This is in marked contrast to the mouse embryo, where the WNT signaling pathway is initially activated in a highly localized manner at the primitive streak on the posterior domain and is strictly regulated by the secretion of WNT antagonists from the anterior visceral endoderm (Arnold and Robertson, 2009). The resulting signal gradient thus protects the anterior epiblast from the “posteriorizing” signals, maintaining it in an uncommitted state (Kimura et al., 2000). In fact, mutated mouse embryos with increased WNT activity upregulate the genes of the posterior mesoderm in the anterior domain (Osteil et al., 2019), which leads to a doubling of the posterior axis (Merrill et al., 2004) and to the failure of anterior brain formation (Fossat et al., 2011; Lewis et al., 2008; Mukhopadhyay et al., 2001).





Based on this understanding, we postulated that the absence of anterior neural tissue in existing gastruloids could be attributed, at least partially, to excessive WNT signaling in the early stages of culture and that, consequently, a decrease in WNT signaling levels in incipient ESC aggregates could promote the emergence of the missing anterior domains in gastruloids. To develop starting conditions that could trigger the formation of gastruloids independently of exogenous stimulation with the WNT agonist CHIR99021, we therefore modified the existing culture medium to obtain more physiological epiblast identity. When aggregated in high-throughput in a novel microcavity array system (Brandenberg et al., 2020) and cultured in epiblast induction (EPI) conditions in the presence of fibroblast growth factor 2 (FGF2) and activin-A, but not CHIR99021, the resulting aggregates were found to initiate T/BRA expression, break symmetry, and undergo axial elongation. Remarkably, in the presence of the small-molecule WNT inhibitor XAV939, the EPI aggregates gave rise to gastruloids with a surprising level of antero-posterior (A-P) development, with a population of SOX1+ and SOX2+ cells in front of the extended T/BRA+ domain. Under these culture conditions, it was found that elongation and patterning efficiency was strictly dependent on initial aggregate size and WNT activity; i.e., smaller aggregates could not maintain elongated morphology and A-P patterning was abrogated without WNT inhibition. Overall, our data show the crucial role of the initial conditions, both in terms of size and cell states of the initial mESC aggregate, in promoting morphogenesis and patterning along the A-P axis. Our approach to gastruloid culture provides a simple and versatile *in vitro* tool for the study of peri-gastrulation development and especially the specification of anterior neural tissue.

RESULTS

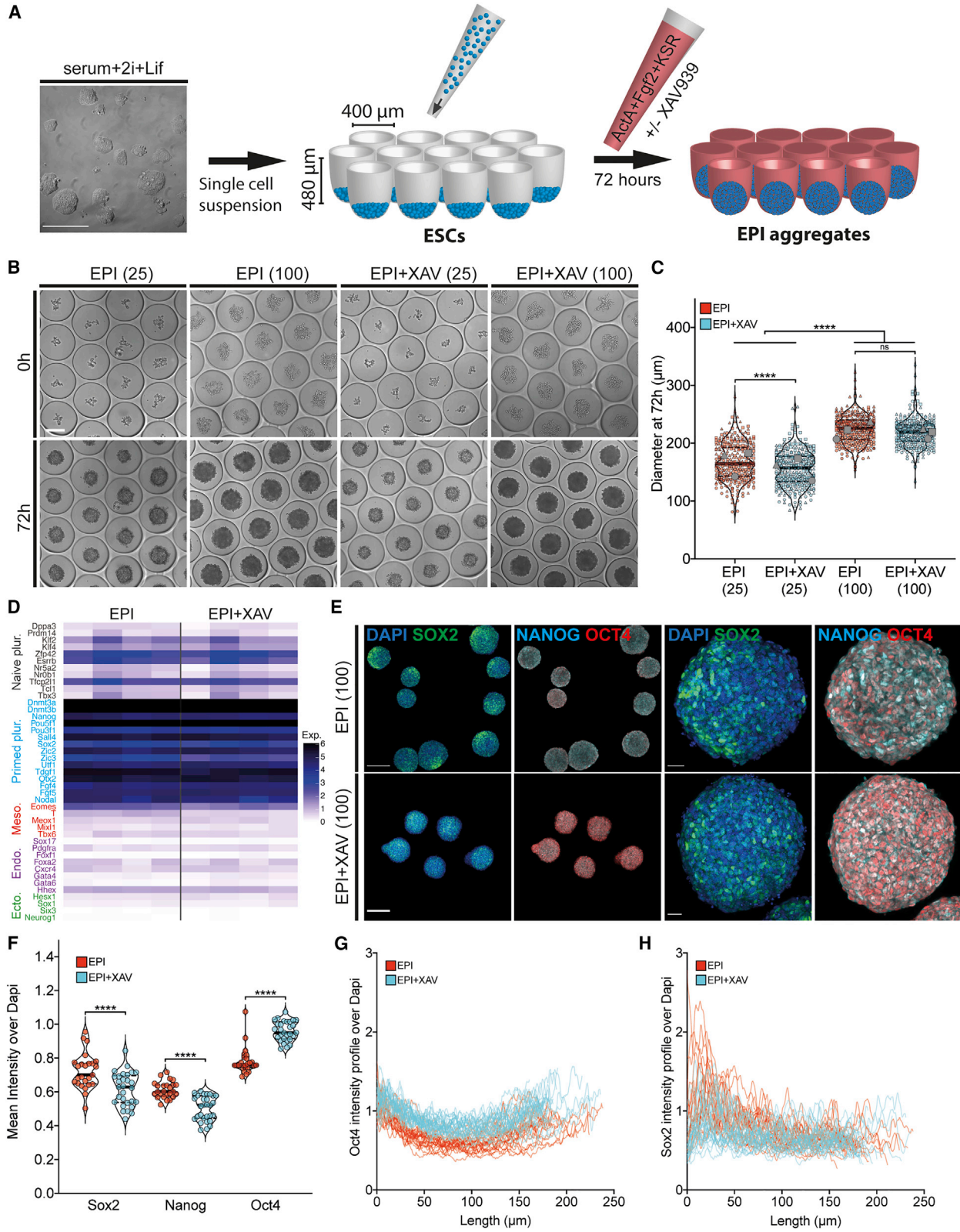
High-throughput formation of EPI aggregates in hydrogel microwells

Because the current gastruloid culture protocol is not conducive to the formation of anterior neural tissues (van den Brink et al., 2014; Turner et al., 2017; Beccari et al., 2018), likely due to premature differentiation toward mesendoderm at the expense of anterior ectoderm, here we modified the existing formulation to promote the formation of “EPI aggregates,” i.e., tissues that could mimic the pluripotent post-implantation epiblast that retains differentiation capacity toward both anterior ectoderm and mesendoderm lineages. We used poly(ethylene glycol) (PEG) microwells to create hundreds of aggregates of the desired size (Brandenberg et al., 2020) (Figures 1A and 1B). To avoid excessive WNT signaling, we removed CHIR99021, and we also added activin-A (20 ng/mL), FGF2 (12 ng/mL), and

knockout serum replacement (1%), thus implementing a medium composition that has previously been shown to induce epiblast identity in mouse ESCs (Hayashi et al., 2011). To achieve a more homogeneous epiblast differentiation, we also supplemented the medium with XAV939, a small-molecule inhibitor of the WNT signaling pathway (Sugimoto et al., 2015; Sumi et al., 2013).

Starting from 25 or 100 cells/well, in both EPI and EPI+XAV media, we successfully created aggregates of different sizes (Figure 1B). Aggregates formed from 100 cells/well in both media had similar average diameters of around 72 h (~220 μm), while aggregates formed from 25 cells/well showed a slightly reduced size when cultured in the presence of XAV939 (~165 versus ~155 μm) (Figure 1C).

Using ESC reporters for WNT (TLC-mCherry) (Ferrer-Vaquer et al., 2010; Faunes et al., 2013) and transforming growth factor β (TGF- β) (AR8-mCherry) (Serup et al., 2012), we next performed time-lapse imaging to gain insight into the dynamics of these signaling pathways during the initial culture period. As expected, WNT+ ESCs cultured in EPI medium gradually lost reporter activity until 48 h, and were slightly upregulated thereafter (Figure S1A). The addition of XAV939 had no effect on the initial rate of WNT downregulation, but upregulation was inhibited after 48 h, resulting in lower levels of WNT activity at around 75 h (Figure S1A). On the contrary, TGF- β signaling was inactive in ESCs and could only be detected in aggregates after 60 h. Interestingly, the addition of XAV939 led to a slightly earlier activation of the TGF- β reporter (Figure S1B). Analysis of pooled aggregates revealed significant reduction of WNT signaling in the presence of XAV939; however, the TGF- β pathway was minimally affected (Figures S1C and S1D). Of note, in both reporter systems we noticed an activation pattern running from the periphery to the center of the 400- μm microwell arrays (Figure S1E). EPI aggregates formed at the periphery of the arrays upregulated the WNT and TGF- β pathways earlier and at higher levels. Differentiating ESCs were shown to secrete DKK1 and LEFTY1 into the paracrine milieu, and higher bulk cell density was associated with limited mesendodermal differentiation (Kempf et al., 2016). A possible explanation could be a reaction-diffusion process in which inhibitors of the WNT and TGF- β pathways were concentrated at the center of the array, thereby limiting reporter activity at the periphery. In support of this hypothesis, such an edge effect was eliminated when aggregates were spaced more distantly in larger wells (800 μm) and all aggregates uniformly activated the WNT and TGF- β reporters (Figure S1F). In neither of the two tested microtiter plate arrays could we detect no T/BRA expression at 72 h. Considering the higher number of aggregates that can be generated, we performed all the subsequent experiments on 400- μm microwell arrays.



(legend on next page)



To confirm that the aggregates have acquired epiblast identity, we performed bulk RNA sequencing comparing EPI aggregates formed with or without XAV939. We found that the majority of the naive pluripotency markers, such as *Rex1* (*Zfp42*), *Klf2/4*, *Esrrb*, *Prdm14*, and *Dppa3* were expressed at low levels. However, primed pluripotency markers, which are expressed in the post-implantation epiblast, such as *Fgf4/5*, *Otx2*, *Sox2*, *Oct4/6* (*Pou5f1/Pou3f1*), and *Nodal* were expressed at high levels, indicating a transition from the naive to the primed state of pluripotency (Ghimire et al., 2018). Moreover, we did not detect expression of differentiation markers toward mesoderm (*T*, *Mixl1*, *Eomes*), endoderm (*Sox17*, *Gata4/6*, *Foxa2*), or ectoderm (*Sox1*, *Six3*, *Neurog1*) lineages, suggesting an undifferentiated state for EPI and EPI+ XAV aggregates (Figure 1D). Furthermore, immunostaining for SOX2, NANOG, and OCT4 confirmed the expression of primed pluripotency factors at the protein level (Figures 1E and 1F). In EPI aggregates formed in the presence of XAV939, we could demonstrate a higher and more homogeneous expression of OCT4, indicating a better maintenance of pluripotency identity with decreased WNT signaling (Kim et al., 2013) (Figures 1F and 1G). Interestingly, we noted a somewhat polarized expression profile of SOX2 in aggregates formed under EPI conditions (Figure 1H). The SOX2+ pole showed an increased WNT and a decreased TGF- β activity, indicating the establishment of an A-P axis similar to that of the 48–72 h gastruloids (Turner et al., 2017) (Figure S1G). On the contrary, in the presence of XAV939, the SOX2 expression was more scattered and the aggregates showed uniform activity for WNT and TGF- β reporters (Figures 1H and S1H). At the level of structural organization, we did not detect lumen formation or epithelial polarization. Instead, the EPI aggregates showed uniform E-CADHERIN expression and had multiple micro-

cavities labeled with phalloidin (Figure S1I). Overall, these results suggest that ESCs could be manipulated to form epiblast-like aggregates in a scalable and reproducible manner, and that the addition of a WNT inhibitor could promote better maintenance of pluripotent epiblast identity.

Axial morphogenesis of EPI aggregates

In conventional gastruloid culture (van den Brink et al., 2014; Turner et al., 2017) mESC aggregates assume an oval shape between 72 and 96 h and continue to elongate for up to 120 h. If the gastruloids are not transferred to shaking culture at this time (Beccari et al., 2018; Girgin et al., 2018), the elongation is not maintained and the gastruloids tend to acquire a rounded shape (Figure 2A). To better understand the dynamics of morphogenesis over time, we performed automated image analysis by fitting a spine to the gastruloids via connecting centers of inscribed circles of different sizes (Figure S2A). We calculated the elongation index by dividing the axial length by the diameter of the largest inscribed circle. This analysis showed a peak value of the elongation index at 120 h, which decreased until 168 h, when the elongated tip collapsed (Figure 2B). However, the gastruloids continued to increase in axial length up to 144 h and reached over 1 mm, suggesting that the loss of elongated morphology was not due to growth inhibition (Figure S2B).

In contrast to classical gastruloids (Turner et al., 2017), when EPI aggregates were placed in low-attachment U-bottomed 96-well plates after 72 h, they were able to elongate autonomously and did not require external WNT stimulation (Figure 2C). The elongation of EPI aggregates showed a strict dependence on the original size of the aggregates. Smaller aggregates (termed EPI(25)) assumed an ovoid shape at 96 h and continued to stretch until 144 h.

Figure 1. Formation of EPI and EPI+ XAV aggregates on PEG microwells

- (A) Schematic showing the experimental method to generate EPI aggregates on PEG microwells from mESCs maintained in s2iL medium.
- (B) Time point images of EPI aggregates formed from 25 and 100 mESCs/well at 0 h (top panel) and 72 h (bottom panel).
- (C) Quantification of the diameter of EPI aggregates at 72 h cultured in indicated conditions. Data are shown as median. N = 3 independent experiments. Total numbers of aggregates analyzed for EPI(25), EPI+ XAV(25), EPI(100) and EPI+ XAV(100) were 312, 335, 315, and 316, respectively.
- (D) Bulk RNA sequencing analysis of EPI and EPI+ XAV aggregates at 72 h formed from 100 cells/well showing expression levels of naive pluripotency, primed pluripotency and early differentiation markers. N = 4 independent experiments.
- (E) Confocal images showing SOX2, NANOG, and OCT4 immunostainings in aggregates cultured under the indicated conditions at 78 h.
- (F) Mean intensity value measurements of SOX2, NANOG, and OCT4 normalized to DAPI intensity. Data are shown as median. Quantification was done on pooled aggregates formed from 100 cells/well from three independent experiments. A total of 25 EPI and 29 EPI+ XAV aggregates was analyzed.
- (G and H) Intensity profiles of OCT4 and SOX2 normalized to DAPI in 78 h aggregates cultured under the indicated conditions. Lines for the intensity profile were drawn from SOX2-high pole through the midline of the aggregates. Quantification was done on pooled aggregates formed from 100 cells/well from three independent experiments. A total of 25 EPI and 29 EPI+ XAV aggregates was analyzed. For statistical analysis, one-way ANOVA followed by Tukey multiple comparison test (C and F) was performed. The following p value style was used for significance: ****p < 0.0001, ***p < 0.0002, **p < 0.0021, *p < 0.0332. Scale bars, 200 μ m. Naive plur., naive pluripotency; Primed plur., primed pluripotency; Meso., mesoderm; Endo., endoderm; Ecto., ectoderm.

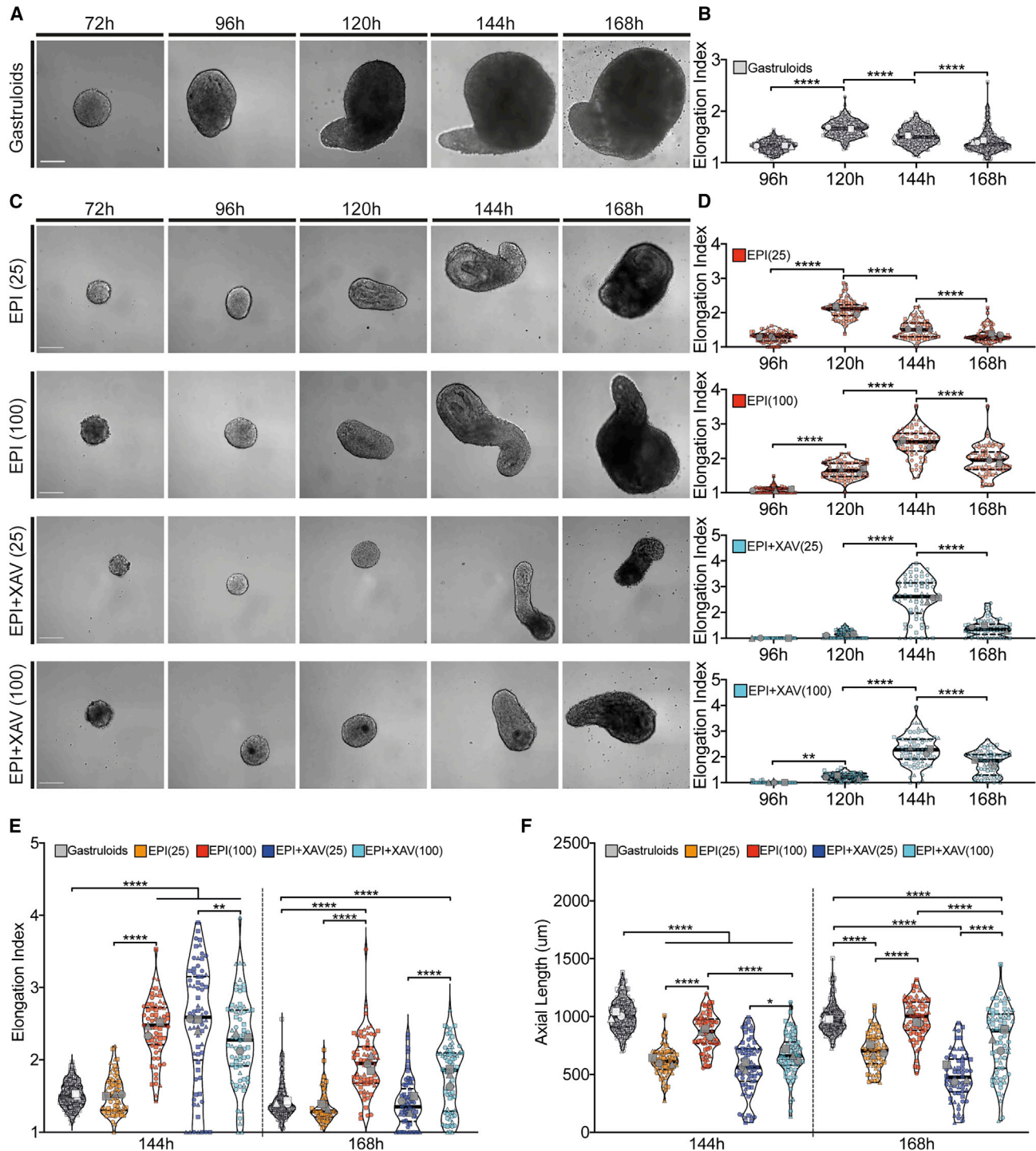


Figure 2. Axial morphogenesis of gastruloids, EPI, and EPI + XAV aggregates

(A) Time point images showing axial elongation dynamics of gastruloids.

(B) Quantification of the elongation index of gastruloids. N = 3 independent experiments. A total of 278 gastruloids were analyzed.

(C) Time point images showing axial elongation dynamics of EPI aggregates cultured under the indicated conditions.

(D) Quantification of the elongation index of EPI aggregates. N = 3 independent experiments. For EPI(25), EPI (100), EPI+ XAV(25), and EPI+ XAV(100) conditions, a total of 72, 66, 71, and 71 aggregates was analyzed.

(legend continued on next page)



In these structures, however, the elongation was not maintained until 168 h because the aggregates gradually rounded off, similar to conventional gastruloids. In contrast, larger EPI aggregates EPI(100) were more roundish at 96 h and started to elongate later, but they maintained a lengthened morphology after 168 h. Surprisingly, in the presence of the WNT inhibitor XAV939 (EPI+ XAV(25)), smaller EPI aggregates did not extend until 120 h, then started to extend massively to 144 h, but could not maintain this morphology until 168 h. However, the effect of initial WNT inhibition was more subtle in larger EPI aggregates (EPI+ XAV(100)) as they were able to maintain an elongated morphology after 168 h (Figures 2C, 2D, and S2C).

The morphological analysis of the EPI aggregates grown under the different conditions confirmed that, after 168 h the aggregates formed from 100 cells/well were significantly more elongated than the aggregates formed from 25 cells/well (Figures 2E and 2F). In comparison with gastruloids, larger EPI aggregates were significantly more elongated, independent of the modulation of WNT activity, but reduced in axial length (Figures 2E and 2F). The addition of XAV939 delayed elongation and limited axial growth, but did not significantly affect the elongation index at 168 h (Figures 2E and 2F). Since focusing on elongation index alone might be misleading (Figure S2D, compare EPI+ XAV(25) with EPI(100)), we selected the 100 cell/well condition, resulting in both high elongation index and axial length, for further characterization. Overall, these results show that EPI aggregates could experience axial elongation even without any exogenous stimulation. It was shown that the temporal elongation dynamics are strictly dependent on the initial aggregate size and WNT activity.

A-P patterning in EPI aggregates

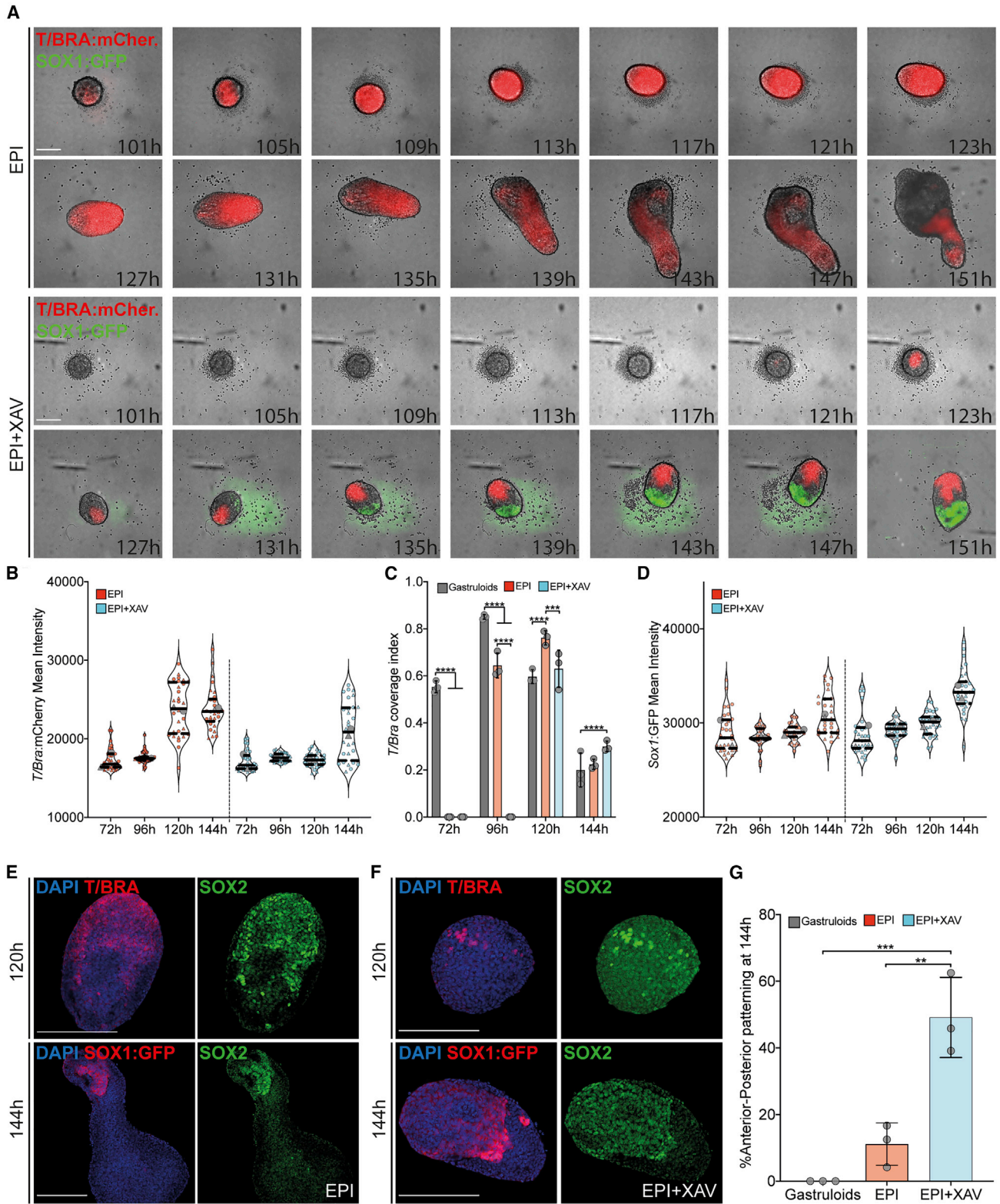
Next, we used time-lapse microscopy to assess the dynamics of symmetry breaking and to monitor the emergence of T/BRA expression in EPI aggregates (Figure 3A, upper panel). Compared with gastruloids (Figures S2E and S2F), T/BRA expression initiation was delayed by 24 h in EPI aggregates. T/BRA expression was increased after 120 h (Figure 3B), covering almost the entire surface of the aggregates (Figure 3C). At this stage, the EPI aggregates showed a pole of T/BRA+ SOX2+ cells, which probably marked neuromesodermal progenitor (NMP) cells at the posterior tail bud of mouse embryos (Henrique et al.,

2015). When EPI aggregates were further cultured until 144 h, the T/BRA+ domain was restricted to the tip, surrounded by SOX1/SOX2-double-positive neuronal tissue similar to the posterior structure in gastruloids (Figures 3E and S2G).

EPI aggregates formed under WNT inhibition (EPI+ XAV) showed a delayed onset of T/BRA expression, starting at low levels around 120 h (Figures 3A, lower panel and 3B). In this case, it was found that the expression domain of T/BRA remained rather localized and did not spread across the entire aggregate (Figure 3C). The T/BRA-negative domain started to express SOX1 (Figure 3A, lower panel) and expression increased up to 144 h (Figure 3D), indicating the formation of neural precursors on the anterior domain of the aggregates. The neural precursors could be detected already after 120 h, as the EPI+ XAV aggregates were uniformly SOX2 positive except for a few highly positive T-BRA/SOX2 NMP cells. At 144 h, the SOX2 expression was polarized to the SOX1+ region located in front of the elongating tip (Figure 3F), an asymmetric pattern profile that we refer to as an A-P pattern. At 144 h, the frequency of A-P patterning was highest in the presence of WNT inhibitor, with $\approx 50\%$ of the aggregates exhibiting posterior T/BRA and anterior SOX1 expression. In contrast, classical gastruloids never showed SOX1-GFP expression anterior to T/BRA, and aggregates formed in EPI medium (i.e., without XAV939) rarely exhibited the phenotype of A-P patterning ($\approx 10\%$) (Figure 3G).

To better understand the role of the key pathways involved in A-P patterning, we used the aforementioned WNT and TGF- β ESC reporter lines to track the pathway dynamics during the development of EPI aggregates. Already at 96–101 h, a low level of WNT signaling was detected, which progressively increased up to 144 h and marked the extended tip (Figures S3A, upper panel and S3C). In some cases, we could detect a smaller WNT+ domain located anteriorly (Figure S3A, white arrowhead). In contrast, TGF- β activity in EPI aggregates was gradually downregulated and limited to the anterior domain (Figures S3A, lower panel and S3D). Overall, the expression patterns of the WNT and TGF- β pathways in EPI aggregates were strikingly similar to those of the gastruloids (Figure S3E). Aggregates formed in EPI+ XAV medium showed a 12–16 h delay in the activation of the WNT pathway, but continued to upregulate WNT to 144 h (Figures S3B, upper panel and S3C). Interestingly, WNT activity in these aggregates was predominantly restricted to the anterior domain

(E and F) Quantification and comparison of elongation index (E) and axial length (F) of gastruloids and EPI aggregates at 144 and 168 h. N = 3 independent experiments. For gastruloids, EPI(25), EPI(100), EPI+ XAV(25), and EPI+ XAV(100) conditions, a total of 278, 72, 66, 71, and 71 aggregates was analyzed. Data are shown as median. Gray symbols indicate mean values of independent experiments. For statistical analysis, one-way ANOVA followed by Tukey multiple comparison test was performed. The following p value style was used for significance: ****p < 0.0001, ***p < 0.0002, **p < 0.0021, *p < 0.0332. Scale bars, 200 μ m.



(legend on next page)



(Figure S3B, upper panel, white arrowhead). Similarly, we observed a general downregulation of the TGF- β signal, but this time along the midline extending to the posterior end (Figures S3B, lower panel and S3D).

At 168 h, the pattern profiles in EPI and EPI+ XAV aggregates were further stabilized. Aggregates formed in the EPI medium showed extended SOX2 expression from 144 h, but still marked up to the “neck” of the extended tip (Figures 4A; white line and S4A). As expected, the posterior neural domain co-expressed SOX1 in the vicinity of the restricted expression of T/BRA at the tip (Figure 4B). Immunostaining for SOX17 and OTX2 showed expression in the anterior epithelia, suggesting the formation of endodermal derivatives (Costello et al., 2015) (Figures 4C and S4B). As expected, the TGF- β signaling pathway was active on the endoderm domain located anterior to the CDX2+ pole (Figures 4D and S4C). The WNT pathway was predominantly active on the extended tail and overlapped with CDX2 expression (Figure S4D). Interestingly, we could not observe the formation of large endodermal pockets in the WNT reporter cell line. In some cases, small WNT+ domains were detected on the anterior domain, organized in epithelial rosettes that were positive for OTX2, probably of neural identity (Figures 4E and S4E).

WNT-inhibited aggregates showed anterior expression of SOX2, which marked tubular epithelia extending from the tip of the tail toward several putative neural rosettes at the anterior end (Figures 4F and S4F, insets). These rosettes were positive for SOX1 (Figure 4G, white arrowhead) and were located adjacent to the SOX17+ OTX2+ endodermal domain, which was much smaller and infrequent than the EPI counterparts (Figures 4H and S4G). Similarly, these small endodermal pockets were positive for TGF- β signaling, which was inactive in adjacent neuronal rosettes (Figures 4I, white arrowhead and S4H, white arrowhead).

WNT signaling marked the anterior domain versus CDX2 (Figure S4I), which was organized in neural rosettes and was positive for OTX2 and EN1, indicating a possible formation of a primitive brain-like region in late-stage EPI+ XAV aggregates (Figures 4J and S4J). Collectively, these data suggest a differential patterning profile of tissues in EPI and EPI+ XAV aggregates at 168 h (Figure S4K).

To better characterize the dynamics of tissue formation in EPI aggregates, we performed time course bulk RNA sequencing from 72 to 168 h. EPI and EPI+XAV aggregates were indistinguishable at the global transcriptomic level at early stages, but we observed the late onset effect of XAV treatment as the aggregates developed further (Figure 4K). We detected an early upregulation of genes expressed in the primitive streak in EPI aggregates by 96 h, which was delayed in XAV-treated aggregates until 120 h. Comparative analysis showed that, after 120 h of culture, the differences in the global transcriptional profiles of EPI and EPI+ XAV aggregates became more evident. Transcripts marking the definitive endoderm and mesoderm derivatives were already increased in EPI aggregates after 120 h, whereas markers of the forebrain/midbrain/hindbrain were conspicuously upregulated in EPI-XAV aggregates (Figure 4L). More detailed analysis of differentially regulated genes revealed that genes involved in heart (*Myl4/7*, *Gata3/4*, *Hand1/2*, *Acta2*, *Ttn*) and intestinal development (*Pyy*, *Cldn7*, *Hnf4a*, *Ap1m2*) were significantly upregulated in EPI aggregates at later stages (Figure 4M). On the other hand, markers of the forebrain (*Foxg1*, *Wnt7b*, *Zic1/4*), midbrain (*En1/2*, *Pax5*, *Otx1*), and hindbrain (*Irx6*, *Pou3f3*, *Msx3*) were more highly expressed in XAV-treated aggregates (Figure 4N).

Taken together, these results suggest that early inhibition of WNT signaling in EPI aggregates could promote formation of anterior neural tissues that comprise a forebrain/midbrain/hindbrain-like identity. The absence of such

Figure 3. Antero-posterior patterning in EPI and EPI+ XAV aggregates at 144 h

(A) Time point images showing T/BRA-mCherry and SOX1-GFP expression dynamics in EPI (top panel) and EPI+ XAV (bottom panel) aggregates.

(B) Quantification of mean T/BRA-mCherry intensity in EPI and EPI+ XAV aggregates until 144 h. N = 2 independent experiments. For each EPI and EPI+ XAV conditions, a total of 36 aggregates was analyzed.

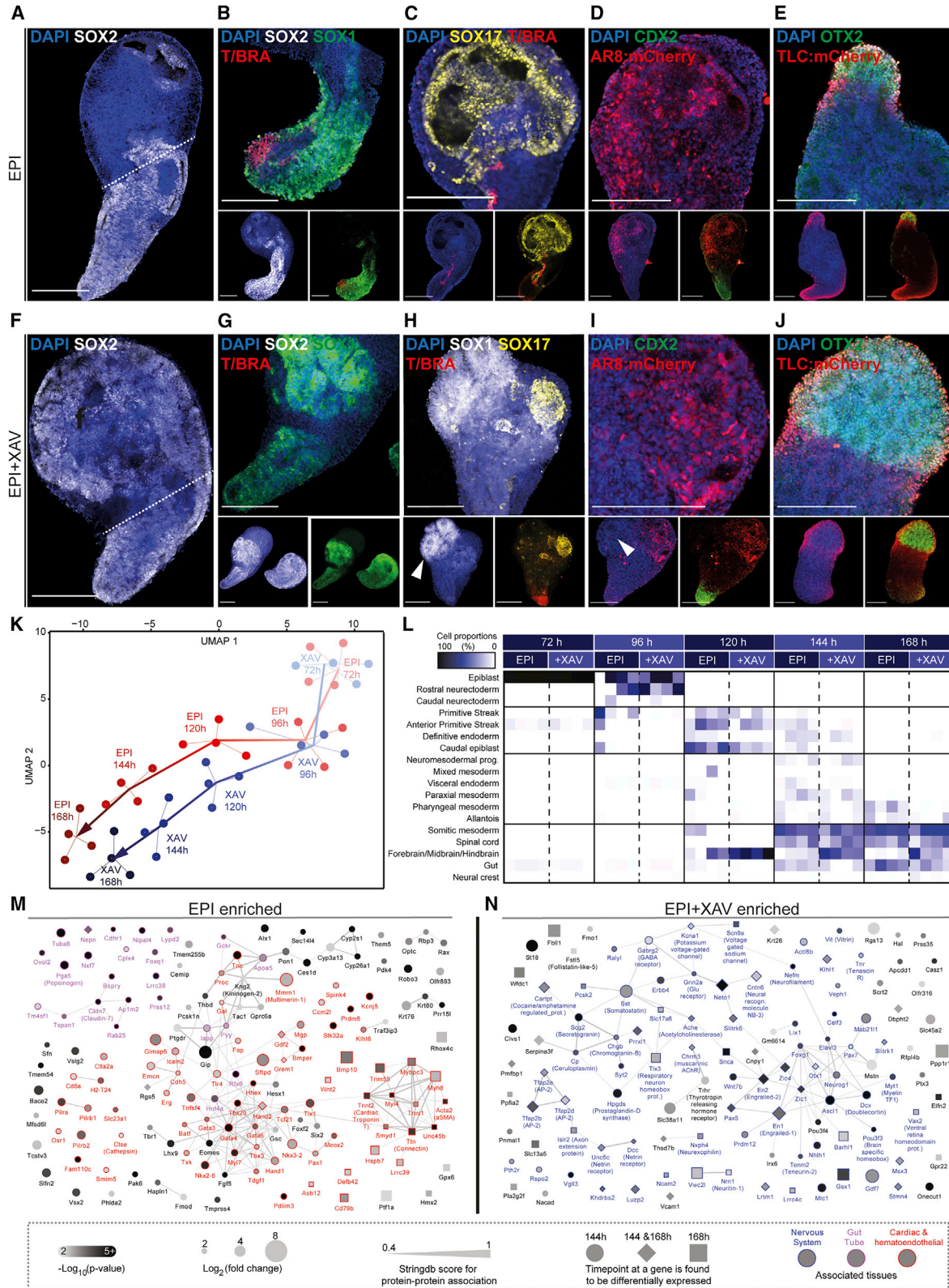
(C) Quantification of T/BRA-mCherry coverage index as calculated by dividing the T/BRA-mCherry+ area to total aggregate area. N = 3 independent experiments. For gastruloids, EPI, and EPI+ XAV conditions, a total of 278, 72, and 71 aggregates was analyzed, respectively.

(D) Quantification of mean SOX1-GFP intensity in EPI and EPI+ XAV aggregates until 144 h. N = 2 independent experiments. For each EPI and EPI+ XAV condition, 36 aggregates were analyzed.

(E) Representative confocal images at 120 and 144 h showing posteriorly localized T/BRA, SOX1, and SOX2 expression in EPI aggregates.

(F) Representative confocal images at 120 and 144 h showing T/BRA and anteriorly localized SOX1 and SOX2 expressions in EPI+ XAV aggregates.

(G) Quantification of antero-posterior patterning frequency in gastruloids, EPI, and EPI+ XAV aggregates described as exhibiting T/BRA and SOX1 expression on the opposite sides. N = 3 independent experiments. For gastruloids, EPI, and EPI+ XAV conditions, a total of 278, 72, and 70 aggregates was analyzed, respectively. Data are shown as median (B and D) or mean with standard deviation (C and G). Gray symbols indicate mean values of independent experiments. For statistical analysis, one-way ANOVA (G) or two-way ANOVA (C) followed by Tukey multiple comparison test was performed. Following p value style was used for significance: ****p < 0.0001, ***p < 0.0002, **p < 0.0021, *p < 0.0332. Scale bars, 200 μ m.



(legend on next page)



tissues in gastruloids and EPI aggregates formed in the absence of WNT inhibition might suggest that anterior neural tissue precursors were probably lost in these structures and replaced by mesendodermal precursors instead, hence they demonstrate more abundant heart-like and gut-like tissues. The addition of XAV939 could probably reverse this effect by maintaining a more homogeneous epiblast identity, as demonstrated by more uniform expression of pluripotency factors and delayed axis specification. In turn, these aggregates could have a much broader differentiation potential and form anterior neural and endodermal tissues composed of neural rosettes and columnar epithelia, respectively.

DISCUSSION

We report on a culture system for the derivation of post-implantation epiblast-like structures by aggregation and pretreatment of ESCs. We formulated a serum-free epiblast induction medium containing activin-A (TGF- β agonist), FGF2 (FGF agonist), and knockout serum substitutes that promoted the acquisition of epiblast identity of ESC aggregates, followed by their spontaneous symmetry breaking and subsequent morphogenesis without any external WNT stimulation. Accordingly, mouse embryos that specifically lack *Wnt3* in the posterior visceral endoderm break symmetry, initiate gastrulation, and form a primitive streak, indicating an autonomous development potential of epiblast cells that is independent of an extra-embryonic WNT source (Yoon et al., 2015). It is conceivable that, in our EPI aggregates, a critical level of WNT signaling is reached by synergistic activities of TGF- β and FGF pathways, as shown previously (Hayashi et al., 2011), which in turn triggers T/BRA expression (Turner et al., 2017; ten Berge et al., 2008). In fact, a TCF/LEF complex reporter

showed endogenous WNT activity in 72 h EPI aggregates, which preceded T/BRA expression and was further expressed until late stages. This could indicate that a WNT signal is required for the elongation of EPI aggregates, analogous to the dependence of epiblast cells on endogenous WNT signals for further development (Tortelote et al., 2013). We have shown that the inhibition of WNT signaling by XAV939 during the first 72 h does not have a significant effect on elongation at later points in time, indicating a dynamic, self-organizing nature of EPI aggregates. Nevertheless, inhibition of the WNT signaling pathway at later stages or at different levels might possibly influence the dynamics of axial elongation by shifting the endogenous WNT activity threshold.

Similar to the gastruloids, EPI aggregates showed a posterior pattern with WNT+ neural tissue localized at the elongating tip (Nordström et al., 2002) and TGF- β + endodermal tissue located at the anterior domain (Tremblay et al., 2000). In accordance with this, we detected limited expression of neural genes and expanded representation of heart- and gut-like tissues at transcript level in late-stage EPI aggregates. This limited neural pattern may be due to the fact that WNT levels in early-stage gastruloids and EPI aggregates are above a threshold that would promote consistent mesendodermal conversion at the expense of anterior neural progenitors. Accordingly, Osteil et al. (2019) showed that embryos with increased WNT activity lose these precursors and replace them with mesoderm derivatives instead. In this work, treatment with the WNT inhibitor IWP2 resulted in a more homogeneous epiblast stem cell population and increased differentiation ability compared with ectodermal derivatives. In our model, early WNT inhibition by XAV939 allowed higher OCT4 levels and a more homogeneous SOX2 expression compared with aggregates cultured only in EPI medium. This could indicate a prolonged pluripotent epiblast identity with an increased

Figure 4. Antero-posterior patterning in EPI and EPI+ XAV aggregates at 168 h

- (A) Confocal image of an EPI aggregate at 168 h immunostained for SOX2.
- (B) Confocal image showing colocalization of SOX1 and SOX2 expression at the posterior neural domain of an EPI aggregate.
- (C) Confocal images showing SOX17 expression at the anterior “endoderm” domain of EPI aggregates at 168 h.
- (D) Confocal images showing mCherry and CDX2 expression in EPI aggregates formed from the AR8-mCherry reporter line.
- (E) Confocal images showing mCherry and “neural” OTX2 expression in EPI aggregates formed from the TLC-mCherry reporter line.
- (F) Confocal image of an EPI+ XAV aggregate at 168 h immunostained for SOX2.
- (G) Confocal image showing colocalization of SOX1 and SOX2 expression at the anterior and posterior neural domain of an EPI+ XAV aggregate.
- (H) Confocal images showing SOX17 expression at the anterior “endoderm” domain of EPI+ XAV aggregates at 168 h.
- (I) Confocal images showing mCherry and CDX2 expression in EPI+ XAV aggregates formed from the AR8-mCherry reporter line.
- (J) Confocal images showing mCherry and “neural” OTX2 expression in EPI+ XAV aggregates formed from the TLC-mCherry reporter line.
- (K) UMAP analysis of bulk RNA-seq datasets using time-pooled EPI and EPI+ XAV aggregates from 72 to 168 h showing differentiation trajectories (n = 4 replicates per time point).
- (L) Heatmap of proportions of different embryonic tissues in pooled EPI and EPI+ XAV aggregates from 72 to 168 h (n = 4 replicates per time point).
- (M and N) Network of differentially expressed genes in EPI (M) or EPI+ XAV (N) aggregates at 144 and 168 h. Scale bars, 200 μ m.



potential for differentiation into both anterior neural and posterior mesendodermal fates. As a result, we observed the occurrence of expanded SOX1+ SOX2+ neural tissues in WNT-inhibited EPI aggregates that were adjacent to SOX17+ endodermal tissue located anterior to the T/BRA-expressing tip. RNA sequencing showed that the neural tissue comprised a brain-like identity, expressing genes that mark the forebrain, midbrain and hindbrain that were collectively missing in gastruloids.

Overall, our work offers a new methodology for studying early embryonic development of the mouse *in vitro* with an extended potential compared with conventional gastruloids. We believe that these second-generation gastruloids could be useful to answer questions focusing on epiblast development and the formation of ectoderm and mesoderm origin tissues. Future work is needed for a more detailed analysis of the cell types that are produced in EPI aggregates. In addition, the addition of extra-embryonic cells could be a useful extension of the model, allowing to study the extent of the self-assembly properties of ESCs of the mouse.

EXPERIMENTAL PROCEDURES

Cell culture

Mouse ESCs (SBr line [SOX1-GFP; T/BRA-mCherry] [Deluz et al., 2016], WNT line [TLC-mCherry] [Faunes et al., 2013; Ferrer-Vaquer et al., 2010], and TGF- β line [AR8-mCherry] [Serup et al., 2012]) were cultured at 37°C in 5% CO₂ in medium composed of DMEM+ Glutamax (no. 61965-026), 10% ESC-qualified FBS (no. 16141-079), 1 mM sodium pyruvate (no. 11360-070), 1 \times MEM non-essential amino acids (no. 11140-035), 0.1 mM 2-mercaptoethanol (no. 31350-010), and 1,000 u/mL Pen/Strep (no. 15140-122) supplemented with 3 μ M GSK3i (no. 361559), 1 μ M MEKi (no. S1036), and 0.1 μ g/mL LIF (in house preparation) (s2iL). Cells were routinely passaged every 2–3 days by seeding 8,000–9,000 cells/cm² and every 20 passages a fresh vial was thawed. Cells were tested and confirmed free of mycoplasma.

Preparing EPI differentiation medium

N2B27 medium was prepared by 1:1 mixing of DMEM/F12+ GlutaMAX (no. 31331-028) and Neurobasal (no. 21103-049) with the addition of 0.5 \times N2 supplement (no. 17502001), 0.5 \times B27 supplement (no. 17504001), 0.5 \times GlutaMAX (no. 35050-038), 1 mM sodium pyruvate (no. 11360-070), 1 \times MEM non-essential amino acids (no. 11140-035), 0.1 mM 2-mercaptoethanol (no. 31350-010), and 1,000 u/mL pen/strep (no. 15140-122); 12 ng/mL FGF2 (no. PMG0035), 20 ng/mL activin-A (no. 338-AC), and 1% KSR (no. 10828-010) were added to make final EPI differentiation medium.

Preparing EPI aggregates on PEG microwells

PEG microwells with 400 μ m well diameter (121 wells per array) were prepared on 24-well plates, as described previously (Brandenberg et al., 2020). Microwells were equilibrated with 50 μ L of either

EPI differentiation medium for 30 min at 37°C. Mouse ESCs were dissociated to single cells with Accutase (no. A11105-01). Cells were then centrifuged at 1,000 rpm for 5 min and washed twice with 10 mL PBS. Cells were resuspended in EPI differentiation medium and the desired cell number per well was further adjusted from the cell suspension. For example, 35 μ L of the 484,000 cells/mL suspension was added dropwise on microwell arrays to have 100–150 cells/well. Seeding was done at 37°C for 20 min. EPI differentiation medium (1 mL) with or without 10 μ M XAV939 (no. 3748) was slowly added from the side of the well. Plates were kept at 37°C in 5% CO₂ for at least 72 h before further processing.

Transferring EPI aggregates to 96-well plates

At 72–80 h of culture, aggregates on microwell arrays were flushed out and transferred to non-tissue culture-treated 10-cm plates in 10 mL warm N2B27 medium with no additional factors. Aggregates located on the periphery of the arrays were slightly bigger than the central ones, therefore single EPI aggregates with a diameter closest to but no more than 220 μ m (for 100 cells/well) were targeted and transferred in 10 μ L to low-adherent U-bottomed 96-well plates (no. COR-7007). N2B27 medium (180 μ L) was added on top. At 96, 120, and 144 h, 150 μ L of medium was replaced with fresh N2B27 and EPI aggregates were kept until 168 h.

Data and code availability

All sequence data are accessible with accession number GEO: GSE171210.

SUPPLEMENTAL INFORMATION

Supplemental information can be found online at <https://doi.org/10.1016/j.stemcr.2021.03.017>.

AUTHOR CONTRIBUTIONS

M.U.G. and M.P.L. conceived the study, designed experiments, analyzed data, and wrote the manuscript. M.U.G. performed the experiments. N.B. analyzed the bulk RNA sequencing data. L.M. helped with experiments and image analysis.

DECLARATION OF INTERESTS

The authors declare no competing interests.

ACKNOWLEDGMENTS

We thank Giuliana Rossi and Alfonso Martinez-Arias for useful feedback on the manuscript. We thank Sylke Hoehnel and Nathalie Brandenberg (SUN biosciences) for providing PEG microwell plates and technical support. We thank members of the Lutolf laboratory for discussions and sharing materials. We thank Romain Guiet and Olivier Burri for providing the image analysis codes, and Arne Seitz and other members of Bioimaging and Optics Facility (EPFL) for microscopy support. We thank all personnel of the Histology Core Facility for their technical support. This work was funded by EPFL.



Received: October 16, 2020

Revised: March 17, 2021

Accepted: March 17, 2021

Published: May 11, 2021

REFERENCES

- Arnold, S.J., and Robertson, E.J. (2009). Making a commitment: cell lineage allocation and axis patterning in the early mouse embryo. *Nat. Rev. Mol. Cell Biol.* *10*, 91–103.
- Bain, G., Kitchens, D., Yao, M., Huettner, J.E., and Gottlieb, D.I. (1995). Embryonic stem cells express neuronal properties in vitro. *Dev. Biol.* *168*, 342–357.
- ten Berge, D., Koole, W., Fuerer, C., Fish, M., Eroglu, E., and Nusse, R. (2008). Wnt signaling mediates self-organization and axis formation in embryoid bodies. *Cell Stem Cell* *3*, 508–518.
- Beccari, L., Moris, N., Girgin, M.U., Turner, D.A., Baillie-Johnson, P., Cossy, A.C., Lutolf, M.P., Duboule, D., and Arias, A.M. (2018). Multi-axial self-organization properties of mouse embryonic stem cells into gastruloids. *Nature* *562*, 272–276.
- Boheler, K.R., Czyz, J., Tweedie, D., Yang, H.T., Anisimov, S.V., and Wobus, A.M. (2002). Differentiation of pluripotent embryonic stem cells into cardiomyocytes. *Circ. Res.* *91*, 189–201.
- van den Brink, S.C., Baillie-Johnson, P., Balayo, T., Hadjantonakis, A.K., Nowotschin, S., Turner, D.A., and Martinez Arias, A. (2014). Symmetry breaking, germ layer specification and axial organisation in aggregates of mouse embryonic stem cells. *Development* *141*, 4231–4242.
- Brandenberg, N., Hoehnel, S., Kuttler, F., Homicsko, K., Ceroni, C., Ringel, T., Gjorevski, N., Schwank, G., Coukos, G., Turcatti, G., and Lutolf, M.P. (2020). High-throughput automated organoid culture via stem-cell aggregation in microcavity arrays. *Nat. Biomed. Eng.* *345*, 1–12.
- Costello, I., Nowotschin, S., Sun, X., Mould, A.W., Hadjantonakis, A.K., Bikoff, E.K., and Robertson, E.J. (2015). Lhx1 functions together with Otx2, Foxa2, and Ldb1 to govern anterior mesendoderm, node, and midline development. *Genes Dev.* *29*, 2108–2122.
- Deluz, C., Friman, E.T., Strebinger, D., Benke, A., Raccaud, M., Calligari, A., Leleu, M., Manley, S., and Suter, D.M. (2016). A role for mitotic bookmarking of SOX2 in pluripotency and differentiation. *Genes Dev.* *30*, 2538–2550.
- Faunes, F., Hayward, P., Descalzo, S.M., Chatterjee, S.S., Balayo, T., Trott, J., Christoforou, A., Ferrer-Vaquer, A., Hadjantonakis, A.K., Dasgupta, R., and Arias, A.M. (2013). A membrane-associated β -catenin/Oct4 complex correlates with ground-state pluripotency in mouse embryonic stem cells. *Development* *140*, 1171–1183.
- Ferrer-Vaquer, A., Piliszek, A., Tian, G., Aho, R.J., Dufort, D., and Hadjantonakis, A.K. (2010). A sensitive and bright single-cell resolution live imaging reporter of Wnt/ β -catenin signaling in the mouse. *BMC Dev. Biol.* *10*, 121–218.
- Fossat, N., Jones, V., Khoo, P.L., Bogani, D., Hardy, A., Steiner, K., Mukhopadhyay, M., Westphal, H., Nolan, P.M., Arkell, R., and Tam, P.P. (2011). Stringent requirement of a proper level of canonical WNT signalling activity for head formation in mouse embryo. *Development* *138*, 667–676.
- Ghimire, S., Van der Jeught, M., Neupane, J., Roost, M.S., Anckaert, J., Popovic, M., Van Nieuwerburgh, F., Mestdagh, P., Vandesompele, J., Deforce, D., et al. (2018). Comparative analysis of naive, primed and ground state pluripotency in mouse embryonic stem cells originating from the same genetic background. *Sci. Rep.* *8*, 5884–5911.
- Girgin, M.U., Baillie-Johnson, P., Turner, D.A., Beccari, L., Moris, N., Cossy, A.C., Lutolf, M.P., Duboule, D., and Martinez-Arias, A. (2018). Generating gastruloids from mouse embryonic stem cells. *Protoc. Exchange* <https://doi.org/10.1038/protex.2018.094>.
- Hayashi, K., Ohta, H., Kurimoto, K., Aramaki, S., and Saitou, M. (2011). Reconstitution of the mouse germ cell specification pathway in culture by pluripotent stem cells. *Cell* *146*, 519–532.
- Henrique, D., Abranches, E., Verrier, L., and Storey, K.G. (2015). Neuromesodermal progenitors and the making of the spinal cord. *Development* *142*, 2864–2875.
- Kempf, H., Olmer, R., Haase, A., Franke, A., Bolesani, E., Schwanke, K., Robles-Diaz, D., Coffee, M., Göhring, G., Dräger, G., et al. (2016). Bulk cell density and Wnt/TGF β signalling regulate mesendodermal patterning of human pluripotent stem cells. *Nat. Commun.* *7*, 13602–13613.
- Kim, H., Wu, J., Ye, S., Tai, C.I., Zhou, X., Yan, H., Li, P., Pera, M., and Ying, Q.L. (2013). Modulation of β -catenin function maintains mouse epiblast stem cell and human embryonic stem cell self-renewal. *Nat. Commun.* *4*, 1–11.
- Kimura, C., Yoshinaga, K., Tian, E., Suzuki, M., Aizawa, S., and Matsuo, I. (2000). Visceral endoderm mediates forebrain development by suppressing posteriorizing signals. *Dev. Biol.* *225*, 304–321.
- Kleinsmith, L.J., and Pierce, G.B. (1964). Multipotentiality of single embryonal carcinoma cells. *Cancer Res.* *24*, 1544–1551.
- Kubo, A., Shinozaki, K., Shannon, J.M., Kouskoff, V., Kennedy, M., Woo, S., Fehling, H.J., and Keller, G. (2004). Development of definitive endoderm from embryonic stem cells in culture. *Development* *131*, 1651–1662.
- Lewis, S.L., Khoo, P.L., De Young, R.A., Steiner, K., Wilcock, C., Mukhopadhyay, M., Westphal, H., Jamieson, R.V., Robb, L., and Tam, P.P. (2008). Dkk1 and Wnt3 interact to control head morphogenesis in the mouse. *Development* *135*, 1791–1801.
- Mallo, M., and Alonso, C.R. (2013). The regulation of Hox gene expression during animal development. *Development* *140*, 3951–3963.
- Martin, G.R., and Evans, M.J. (1975). Differentiation of clonal lines of teratocarcinoma cells: formation of embryoid bodies in vitro. *Proc. Natl. Acad. Sci. U S A* *72*, 1441–1445.
- Merrill, B.J., Pasolli, H.A., Polak, L., Rendl, M., García-García, M.J., Anderson, K.V., and Fuchs, E. (2004). Tcf3: a transcriptional regulator of axis induction in the early embryo. *Development* *131*, 263–274.
- Mukhopadhyay, M., Shtrom, S., Rodriguez-Esteban, C., Chen, L., Tsukui, T., Gomer, L., Dorward, D.W., Glinka, A., Grinberg, A., Huang, S.P., et al. (2001). Dickkopf1 is required for embryonic head induction and limb morphogenesis in the mouse. *Dev. Cell* *1*, 423–434.



- Nordström, U., Jessell, T.M., and Edlund, T. (2002). Progressive induction of caudal neural character by graded Wnt signaling. *Nat. Neurosci.* *5*, 525–532.
- Osteil, P., Studdert, J.B., Goh, H.N., Wilkie, E.E., Fan, X., Khoo, P.L., Peng, G., Salehin, N., Knowles, H., Han, J.J., et al. (2019). Dynamics of Wnt activity on the acquisition of ectoderm potency in epiblast stem cells. *Development* *146*, dev172858.
- Serup, P., Gustavsen, C., Klein, T., Potter, L.A., Lin, R., Mullapudi, N., Wandzioch, E., Hines, A., Davis, A., Bruun, C., et al. (2012). Partial promoter substitutions generating transcriptional sentinels of diverse signaling pathways in embryonic stem cells and mice. *Dis. Model Mech.* *5*, 956–966.
- Sugimoto, M., Kondo, M., Koga, Y., Shiura, H., Ikeda, R., Hirose, M., Ogura, A., Murakami, A., Yoshiki, A., Chuva de Sousa Lopes, S.M., and Abe, K. (2015). A simple and robust method for establishing homogeneous mouse epiblast stem cell lines by Wnt inhibition. *Stem Cell Rep.* *4*, 744–757.
- Sumi, T., Oki, S., Kitajima, K., and Meno, C. (2013). Epiblast ground state is controlled by canonical Wnt/ β -catenin signaling in the postimplantation mouse embryo and epiblast stem cells. *Q. Wu*, ed. *8*, e63378.
- Tortelote, G.G., Hernández-Hernández, J.M., Quaresma, A.J., Nickerson, J.A., Imbalzano, A.N., and Rivera-Pérez, J.A. (2013). Wnt3 function in the epiblast is required for the maintenance but not the initiation of gastrulation in mice. *Dev. Biol.* *374*, 164–173.
- Tremblay, K.D., Hoodless, P.A., Bikoff, E.K., and Robertson, E.J. (2000). Formation of the definitive endoderm in mouse is a Smad2-dependent process. *Development* *127*, 3079–3090.
- Turner, D.A., Girgin, M., Alonso-Crisostomo, L., Trivedi, V., Baillie-Johnson, P., Glodowski, C.R., Hayward, P.C., Collignon, J., Gustavsen, C., Serup, P., et al. (2017). Anteroposterior polarity and elongation in the absence of extra-embryonic tissues and of spatially localised signalling in gastruloids: mammalian embryonic organoids. *Development* *144*, 3894–3906.
- Yoon, Y., Huang, T., Tortelote, G.G., Wakamiya, M., Hadjantonakis, A.K., Behringer, R.R., and Rivera-Pérez, J.A. (2015). Extra-embryonic Wnt3 regulates the establishment of the primitive streak in mice. *Dev. Biol.* *403*, 80–88.